Letter

Ordering hard-sphere particle suspensions by medium crystallization: Effect of size and interaction strength

Vianney Gimenez-Pinto*

Department of Chemical Engineering, Columbia University, New York, New York 10027, USA

(Received 27 December 2021; accepted 17 January 2022; published 3 March 2022)

While microstructure in soft materials is usually given by the self-assembly of their constituting building blocks, colloidal assembly can also be obtained via templating a morphology in a disordered suspension of particles by solidification of the melt. This order-templating process is applicable to different soft-matter systems with a variety of characteristic length scales, including particle suspensions in water, liquid-crystal materials, and polymer melts. In this work, we numerically investigate the effect of particle size and solvent size in the process of solidification templating by implementing a coarse-grain model of hard-sphere particles at a moving melt–crystal interface. This approach captures the dependence of crystallization templating on speed of crystal growth, showing the existence of a threshold speed for crystallization templating to occur. Results in this work show that the threshold speed changes following a power form as solvent size and particle size change. Furthermore, this work analyzes and reports the effect of particle–crystal interaction strength in combination with size effects. This scaling study from a numerical perspective sets a starting point for the development of hybrid soft materials via structural templating, allowing solidification-driven particle ordering in different systems with a variety of length scales.

DOI: 10.1103/PhysRevE.105.L032601

I. INTRODUCTION

Advanced soft materials possess an intrinsic capability for creating complex microstructures that can directly affect material macroscopic properties. Consequently, achieving structural order of otherwise disordered particles remains a significant goal for the development and optimization of soft composite materials. Self-assembly in soft matter is commonly due to intrinsic properties of the systems' building units, such as geometry and interaction type. This characteristic behavior exists in liquid-crystal materials [1], colloids, specific polymer-nanocomposite systems [2–4], and beyond [5]. Nonetheless, structural ordering and assembly in a soft material can be engineered via different methods than the intrinsic self-assembly of its constituent's building blocks.

In the case of ice templating or freeze casting, a dispersed suspension of colloidal particles in water can form scaffolds on the order of micrometers and centimeters due to water crystallization. Analog phenomena have been reported in polymer nanocomposites under isothermal crystallization; nanocolloids can be organized to form structures ranging from centimeters [6] to scales as fine as a few tens of nanometers [7]. Beyond the growth of crystals and semicrystals, several studies show that nucleation and growth of a nematic liquid crystal phase can also organize nanoparticles initially dispersed in the isotropic phase. This liquid-crystal templating produces a variety of structures including open cellular [8–10], closed-cell foam, hollow-shell capsules, and branching tubular network [11], based on nematic nucleation and phase separation. Given the variety of systems that can template order in a suspension of particles via melt's phase transitions, and the variety of particle sizes suitable for applications, there is a need to further investigate this mechanism of order templating in particle dispersions and its dependence on size. While crystallization-templating has been implemented vastly in metallurgy and materials science, there is no record in the literature of a study on the size effects of translating the templating process from one system to another.

The present work numerically investigates this templated particle ordering and its size dependence by considering particle kinetics near the edge of a growing crystal, in a similar manner to an ice-templating process. The model considers hard-sphere particles dispersed in a melt, while a crystalline front grows (moves) with a set speed G. Such simplified models are widely implemented in the study of ice templating [12–14]. Yet, they are extensible to other applicable systems. For example, they have demonstrated the ordering of nanoparticles in a polymer-nanoparticle composite due to polymer crystallization [7]. This approach is valid for systems within a regime of optimal particle loading for structural templating, which means particle loading is low and/or particles do not affect the process of solidification (crystallization) of the medium. Such regime has been reported in studies in polymer-nanoparticle dispersions [7] and liquid-crystal colloids [8,11]: particles in a medium that undergoes a phase transition can maintain the phase-transition process qualitatively unchanged while only affecting the transition temperature. In previous

*Present address: Department of Science, Technology and Mathematics, Lincoln University of Missouri, Jefferson City, Missouri 65101, USA; gimenez-pintov@lincolnu.edu

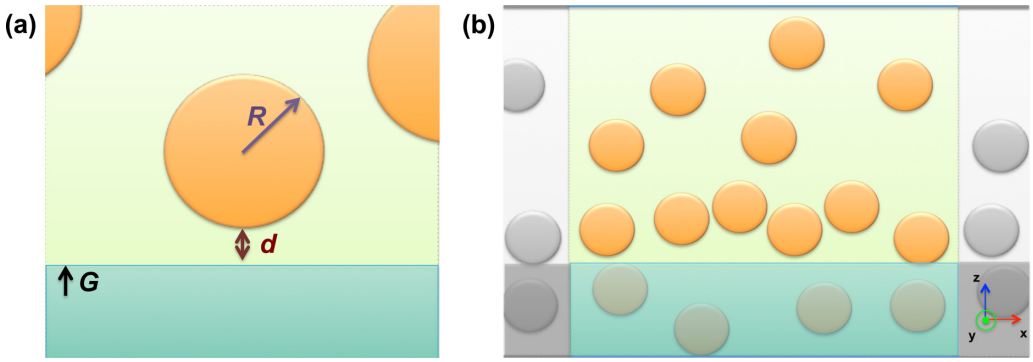

FIG. 1. Model schematics. (a) Single-particle view of the particle-melt-crystal system. Blue area is the crystal front moving with velocity G. Distance d *is* measured from the surface of the melt-immersed particle to the crystal front, and R represents particle radius. (b) Set of n hard-sphere particles in the presence of a moving crystallization front, as simulated in this work. Melt modeling is implicit via viscous drag, average intermolecular distance (solvent size) is present in the van der Waals repulsion, and intrinsic interaction of the crystal-melt-particle system is encoded in the Hamaker constant. Simulation box has periodic boundary conditions in the x- and y axes (only x direction is shown here in grayscale for clarity) and fixed boundaries in z-axis. Particles inside the blue area are engulfed by the crystal, while the rest of particles are free to move and rearrange.

work, we used this ice-templating simulation model to analyze the multiscale ordering of polymethyl methacrylate grafted silica (PMMA-g-silica) nanoparticles in a polyethylene oxide (PEO) melt under regime II crystallization [7]. However, given that order-templating processes transcend the limits of specific systems, presenting a size-dependence analysis in an unlabeled system becomes valuable in this work. Here, the templating process is characterized on the basis of one kinetic parameter: the speed G of the growing crystal. Changing particle size and/or average intermolecular distance in the melt (solvent size) changes particle mobility and affects the overall system's kinetics, including the crystal speed necessary to template order in the surrounding particles. We define a threshold crystal speed G_c for order templating and study how this threshold changes with size and strength of interaction. Careful analysis of results shows a power-form dependence when solvent size varies. Simulations varying particle size also give a power-form dependence showing the effect of changes in particle mass. Furthermore, our study reveals a nonlinear dependence on the particle-crystal interaction strength, embedded in the Hamaker constant. We demonstrate the effect of a few key system parameters such as particle size, average intermolecular distance in the melt (solvent size), and interaction strength (Hamaker constant), when translating the order-templating process between different hard-sphere systems.

II. MODEL

Templating a structure in a material via solidification at a specific rate G depends on the dynamics at the interface between melt and growing crystal [12,13]. At the single-particle level [Fig. 1(a)], a melt-immersed hard particle of radius R, at a distance d between particle surface and crystal edge is subject to an interplay between van der Waals repulsion from the crystal and viscous drag by the medium. van der Waals force follows $F_{vdW} = \Delta\sigma_0(\frac{a_0}{d})^n$ where $n = 4$, $\Delta\sigma_0$ is the surface tension and a_0 the average intermolecular distance in the melt also known as solvent size. F_{vdW} does not explicitly describe the crystal lattice of the growing crystal. Yet, the effect of this factor is embedded in the surface tension, $\Delta\sigma_0(A,\ R,\ a_0) = -\frac{2}{3a_0}\frac{AR}{4a_0+R}$, via the Hamaker constant A characterizing the crystal-melt-particle system. Viscous drag follows $F_{vis} = 6\pi R\eta v$, with η the medium viscosity and v the particle velocity. Note that this approach represents the solvent *implicitly* via Stokes drag and a defined viscosity parameter, while the quantity describing solvent size a_0 is part of the conservative van der Waals force.

When the particle is in the immediate vicinity of the crystal front, particle velocities are evaluated, and the event is analyzed as a collision. If particle velocity ahead of a front is faster than the crystallization speed, the particle will continue moving bounded to the crystal border. Otherwise, the particle is engulfed: the crystalline border moves ahead of the particle and freezes particle movement. Thus, particle ordering depends both *on crystallization speed* G as well as *particle mobility*. For slow crystallization rates, particles have time to respond, move, rearrange, and adopt the morphology of the growing front. At faster crystallization speeds, the crystalline front freezes particle movement and grows ahead of its center of mass, engulfing the particle. During the templating process, particles near the crystal edge can be in direct contact with the crystal surface. If the front does not surpass the particles' position, these particles will be in the grain boundaries of the final crystalline superstructure, adopting its corresponding morphology and length scale.

Under this model, a set of n hard-sphere particles in the presence of a solidification process with speed G [Fig. 1(b)] would adopt the morphology and length scale of the growing crystal for $G < G_c$. On the other side, particles will remain in a dispersed state similar to their initial disordered state for $G > G_c$—Supplemental Material, Fig. S1 [15]. The threshold speed G_c depends strongly on particle mobility within the system. This approach can describe inertial dominated regimes and systems where the assumption of dynamic force equilibrium is not appropriate. Such intuitive toy model of the melt–solid interface allows studying relevant parameters

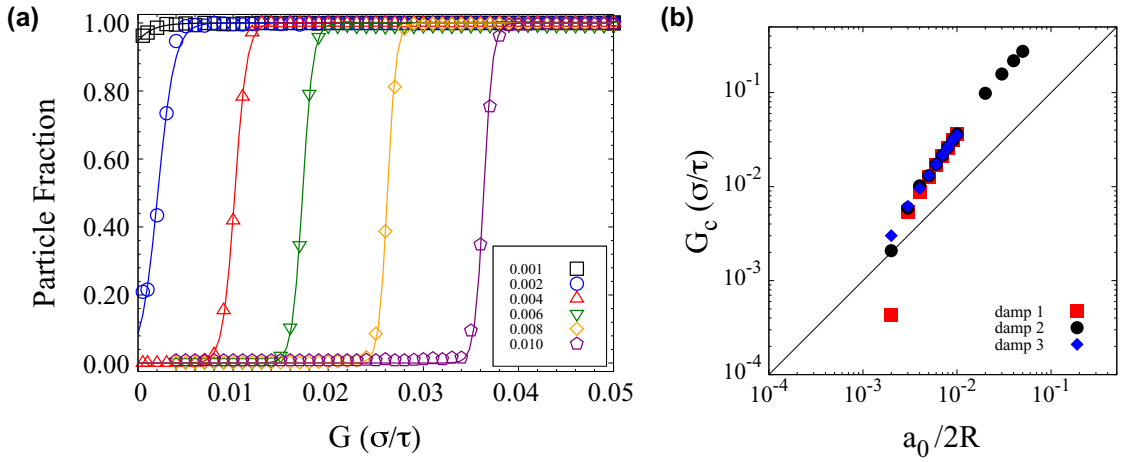

FIG. 2. Particle order by crystallization: Solvent size. (a) Fraction of engulfed particles vs G, damping follows $m/\Gamma = 100.0$. Each data point is an average over five runs of 128 particles with a single growing front. Here particle size follows $2R = 1.0\sigma$ and Hamaker constant is $A = -0.4\varepsilon$. (b) Solvent size run, critical velocity $G_c = -\beta/a$ as a function of $a/2R$ size for damp 1 ($m/\Gamma = 34.0$), damp 2($m/\Gamma = 100.0$), and damp 3 ($m/\Gamma = 340.0$). Tested damping coefficients only show different behaviors when $a/2R < 0.002$. Data are presented in LJ units, common in MD simulations.

for templating fine microstructures in a composite material such as surface tension, particle size, solvent size, medium viscosity and interparticle interactions.

III. METHODS

Molecular dynamics (MD) simulations [16] were carried out in a system of 128 particles interacting with a single growing crystalline front represented by a repulsive moving wall, an approach in the style of Barr *et al.* [14]. Particle-particle interactions are given by a truncated and shifted Lennard-Jones (LJ) potential; solvent and medium are implicitly modeled following Stokes drag Γv with stochastic forces $\zeta(t)$; and crystal-particle interactions follow $F_{vdW} = \Delta\sigma_0(\frac{a_0}{d})^n = -\frac{2}{3a_0}\frac{AR}{4a_0+R}(\frac{a_0}{d})^4$. This expression derives from the van der Waals force $F'_{vdW} = \frac{2}{3}A\frac{R^3}{d(R+d)^2(R+2d)}$ reported by Langbein [17]. Surface tension follows $\Delta\sigma_0(A,\ R,\ a_0) = -\frac{2}{3a_0}\frac{AR}{4a_0+R}$, which we obtain by analyzing the case $d < R$ in F_{vdW}, considering up to the linear terms of d/R and then setting the minimum distance between front and particle to be the solvent size a_0. Kinetic engulfment is applied as described earlier and it is evaluated when $d < 0.05\sigma$. The particles' equation of motion is $F_{net} = -\frac{\partial H}{\partial r} - \Gamma v + \zeta(t)$, which is integrated via the velocity-Verlet algorithm. The simulation box is a square of size 20σ. Boundary conditions are periodic in the x- and y axes, and fixed in the z axis (direction of crystal grow). Particles' forces, velocities, and positions are monitored for different crystallization speeds G. Parameters are expressed in LJ units (σ, ε, τ). Unit conversion to lab units follows σ = distance between particles' centers when the energy is minimum (particle diameter), ε = depth of potential well, and $\tau = \sqrt{\frac{\varepsilon}{m\sigma^2}}$ is a reduced LJ time, m = particle mass. In the initial state, particles are randomly located in the simulation box. Each data point represents an average over five runs. Our use of the term "hard sphere" refers to analyzing colloidal suspensions that behave as hard spheres, not to the use of a full hard-sphere MD potential. Hard-sphere colloids do not attract, or interact, at long ranges, which is captured by a truncated and shifted LJ potential.

IV. EFFECT OF THE SOLVENT SIZE

Figure 2(a) shows the fraction of engulfed particles as a function of crystallization speed for different solvent sizes $a_0 = 0.001$–0.010σ. The engulfment curve shifts to larger velocities as solvent size increases and its behavior can be well described by the function $f(x) = \frac{\tanh(\alpha x+\beta)-1}{2}$, where α and β are fitting parameters that determine threshold velocity as $G_c = -\beta/\alpha$. While any specific point within the transition between order and engulfment can be set as a reference, in this work *the critical velocity* G_c *for particle engulfment is defined as the growth rate where half of the particles in the system are engulfed by a single infinite planar front*. Figure 2(b) shows threshold speeds obtained while varying solvent size. While the relation could be estimated as linear, a detailed analysis shows the data well fit *a power function* $g(a) = ca^b + d$—find fitting parameters in Supplemental Material, Table S1 [15]. Remarkably, the dependence of the critical velocity with solvent size presents an exponent of 4/3.

Figure 2(b) shows G_c vs solvent size within the range $2 \times 10^{-3} < a_0/2R < 1 \times 10^{-2}$. Such strong dependence of G_c on solvent size is a reasonable result: increasing the average intermolecular distance in an unstructured melt allows further particle displacement ahead of the front and raises G_c. For $a_0 < a_{KT} \sim 0.0015\sigma$, our model predicts that thermal fluctuations dominate and produce engulfment of all particles. Effect of the Stokes viscosity η parameter seems minimal compared to the effect of small variations in melt solvent size. The latter can drive the system from a regime of full engulfment to particle reordering, indicating the challenge for experimentally achieving tunable structural templating by crystallization in nanoparticle systems.

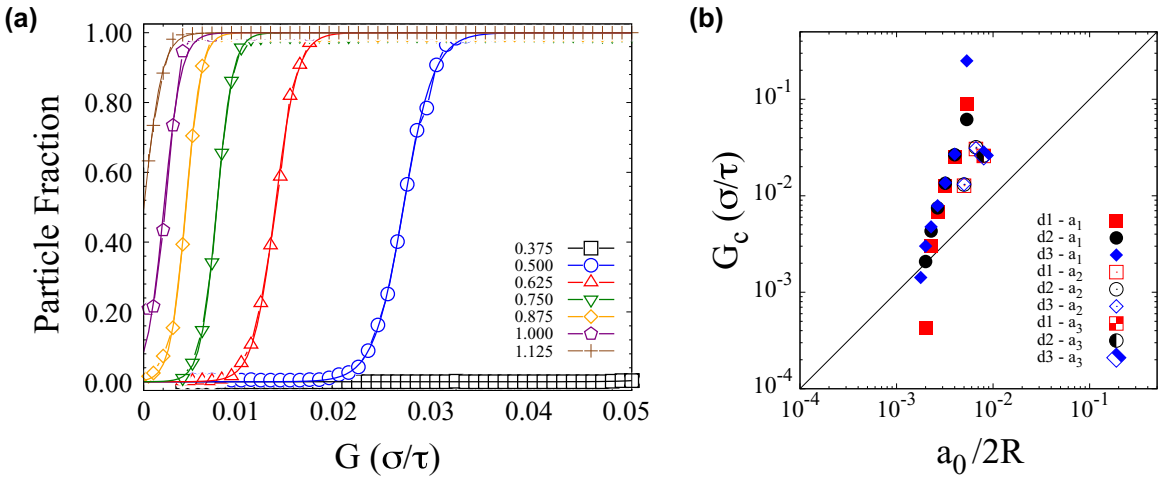

FIG. 3. Particle order by crystallization: Particle size. (a) Fraction of engulfed particles as a function of growth velocity G. Engulfment shifts to larger velocities as particle size decreases. Also, data show a slight softening of the transition with decreasing particle size, noticeable in the $2R = 0.5\sigma$ dataset. (b) Critical velocity G_c vs the inverse of particle size. Shown data for solvent sizes $a_0 = 0.002$, 0.005, and 0.008σ. Damping coefficients are set to match Stokes viscosities for damp 1, damp 2, and damp 3 cases of the reference system $2R_{\text{ref}} = 1.0\sigma$.

V. EFFECT OF THE PARTICLE SIZE

We also evaluate the threshold for engulfment depending on particle size, finding an expected increase in the threshold velocity when particle radius decreases. As particle mobility decreases with particle size, larger front velocities are needed for reaching engulfment. Figure 3(a) shows the fraction of engulfed particles as a function of crystal growth for particle sizes $2R = 0.375$, 0.500, 0.625, 0.750, 0.875, 1.000, and 1.125σ. Figure 3(b) shows the critical velocity ($G_c = -(\alpha/\beta)$) found in simulations varying particle size on melts with different solvent sizes, $a_0 = 0.002$, 0.005, and 0.008σ. Particle mass is modified according to $m = m_{\text{ref}}(R/R_{\text{ref}})^3$ so the density of the particle's material is the same. Also, the damping parameter in the viscous force is modified to maintain the same Stokes viscosity as damp 1, damp 2, and damp 3 systems reported in the solvent size study. Box size and potential cutoff parameters are changed to maintain the same percent particle loading as the solvent size study. Data clearly show that the *dependence of* G_c *with particle size is not linear*, following *an exponential power form*—-fitting parameters and exponents shown in Supplemental Material, Table S2 [15]. There is a limited set of threshold points for $a_0 = 0.008$ and 0.005σ, given the range of parameters selected for comparison with $a_0 = 0.002\sigma$ simulations. Further work with runs aiming at larger speeds can provide more data points. Within the tested range of Stokes-like viscosity parameters, there is no significant variation in G_c. However, two data points show a different behavior when varying η. These correspond with large particles in the damp 1 system ($m/\Gamma = 34.0$) and small particles in the damp 3 system ($m/\Gamma = 340.0$); such points are the smallest and largest G_c values shown in Fig 3(b).

VI. CHANGING MATERIAL INTERACTION STRENGTH AND ITS SIZE EFFECTS

An important factor in the order-templating process is the system-intrinsic strength of interaction given the particles, the melt, and the growing crystalline front. In the present study, this is fully encoded in the van der Waals interaction via the Hamaker constant A, which depends on the material dielectric constants for particles, melted medium, and crystalline front. Changing the system's materials (or crystal lattice) tunes the interaction strength in the particle-melt-crystal system. This is equivalent to changing the magnitude of the repulsive force between the particle and crystalline front, which is a key component when implementing order templating across different systems.

Thus, it becomes important to evaluate the effect of the system-specific Hamaker constant in G_c and how this behavior changes with size. For this, we monitor particle engulfment while varying the Hamaker constant within three orders of magnitude, $A = 0.05$, 0.1, 0.2, 0.4, 0.8, 1.6, and 3.2ε, in systems with solvent sizes $a_0 = 0.002$, 0.006, and 0.010σ. Within this combined study on interaction strength and size effects, data capture final states that span from full particle engulfment to complete particle ordering for all tested crystallization speeds G. This shows that *not all systems template order within their possible speeds of crystallization*. At the same time, *some systems that do display order templating do not exhibit particle engulfment by the growing phase transition given their specific rates for growth*.

A specific subset of simulations presents the threshold between particle ordering and engulfment. Figure 4 shows the threshold velocities found in the current study as a function of the Hamaker constant with different solvent sizes. Results show a general *increase of the threshold speed* G_c as the Hamaker constant A increases. Moreover, *changes in the solvent size rescale this behavior* from a power form, as observed in $a_0 = 0.002$ and 0.006σ, to an apparently linear data set for $a_0 = 0.010\sigma$ within the collected points reported here. Further studies are necessary to fully demonstrate this tendency to linearity in the dependence of G_c with the Hamaker constant, as solvent size increases. In the light of these results, the threshold for solidification templating can be efficiently tuned by considering the combined effect of solvent size and the system-dependent Hamaker constant.

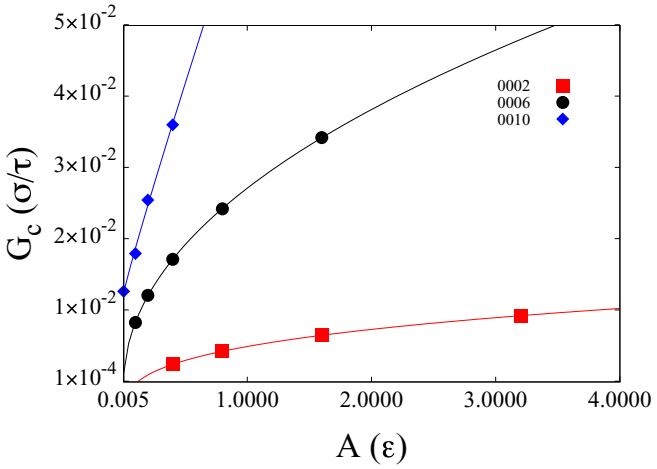

FIG. 4. G_c vs Hamaker constant for different solvent sizes, $a_0 = 0.002$, 0.006, and 0.010σ. The solvent size effect rescales the nonlinear dependence of the critical velocity with the system-intrinsic interaction strength. Lines show fittings to a power form. Supplemental Material, Table S3 [15] shows fitting parameters and exponents obtained.

A few aspects were carefully considered in this work. For example, the Stokes-Einstein relation can miscalculate viscosity for a system with particles of size $\leqslant$10 nm in a polymer melt [18]. Therefore, the application of this study to polymer-nanocomposite systems is only suitable (considering quantitative accuracy) above such size range. Near-interface kinetic studies commonly implement a lubrication form of the Stokes drag, affecting particle mobility and its size dependence. On the other hand, this lubrication limit can overestimate viscous drag, leading to artificial zero-force regimes near the front; this is avoided by implementing a simple Stokes drag [12]. Considering the interest in systems with optimal particle loading for structure templating, this work does not explicitly address the dependence of G on particle concentration. Further work incorporating such self-consistency can model a richer behavior span.

Overall, the critical velocity for particle engulfment increases by increasing the average intermolecular distance in the melt or by decreasing particle size. Both factors increase particle mobility and thus affect the solidification-templating process. Particle size data show a dramatic exponential behavior compared to the solvent size run due to the inclusion of changes in particle mass m. Studies show similar behavior with exponent $4/3$ when particle size data are normalized by $m^{1/3} \sim 2R$, which points us to consider that variations in the components' mass and the density of the solution have an effect on the size dependence of G_c. Remarkably, a $4/3$ nonlinear exponent consistently appears, which could be caused by nonaccounted changes in solvent mass and solution density when solvent size varies with a fixed particle size (solvent size study) or varying particle size and simulation box with a fixed solvent size (particle size study). Thus, considering changes in the density of particles in the solution ρ_R as well as changes in the density of the solvent $\rho_{0,}$ becomes important. By setting an additional term describing the ratio of these densities as $(\rho_0/\rho_R)^{1/3}$, the size dependence of the threshold velocity for particle engulfment trails a form $G_c \quad \frac{1}{2R}(\frac{a_0}{2R})^2$, with a ratio between solvent and particle sizes following a power of 2. Further work for an accurate evaluation of this postulated mass-density effect and factor requires the implementation of an explicit solvent in the model, e.g., dissipative particle dynamics. This would allow a proper evaluation of changes in solution density and solvent mass, as well as its overall effect in the threshold velocity for solidification templating. Also, studies including hydrodynamics effects can be performed via implementing an explicit solvent approach. An explicit model for solvent crystallization can also evaluate the effect of the growing front's crystallographic plane in the ordering process.

The results and coarse-grain model presented in this Letter demonstrate how both particle and solvent size affect main interactions at the moving melt–crystal interface, with effects on particle kinetics and the order-templating process. The threshold velocity for particle engulfment depends on solvent size and trails a power form. Simulations show that small variations in the average intermolecular distance in the melt can drive the system from full engulfment to complete organization. As solvent size decreases below a value a_{KT}, thermal fluctuations become significant to drive full particle engulfment. The dependence of the critical velocity with particle size is also nonlinear and follows a power form. Results show that system-intrinsic interaction strength also presents a strong effect in G_c. Thus, considering the combined effect of size and Hamaker constant is a valuable approach when applying order templating in different systems. In summary, this study has demonstrated that changing particle mobility by size effects takes an essential role in structural templating of soft composite materials by solidification. Results show that both particle and solvent size affect threshold velocity in a nonlinear manner. This realization provides a starting point for an alternate avenue in the development of soft composite materials with structural-driven macroscopic properties.

ACKNOWLEDGMENTS

V.G.-P. thanks Dan Zhao and Jacques Jestin for productive scientific conversations. V.G.-P. also acknowledges Sanat Kumar for valuable guidance in the development of this study, Mayank Misra for initial assistance with molecular dynamics software, as well as the hospitality of the Data Science Institute, Columbia University where this work was performed. Research-computing resources provided by Columbia University Information Technology – CUIT. V.G.-P. acknowledges the hospitality and scholarly resources by the Department of Physics, Temple University, and the Department of Physics and Astronomy, University of Pennsylvania, while writing part of this manuscript. This work was funded by the National Science Foundation Grant No. DMR-1408323.

[1] A. M. Figueiredo Neto and S. R. A. Salinas, *The Physics of Lyotropic Liquid Crystals: Phase Transitions and Structural Properties* (Oxford University Press, New York, 2005).

[2] R. M. Choueiri, E. Galati, H. Thérien-Aubin, A. Klinkova, E. M. Larin, A. Querejeta-Fernández, L. Han, H. L. Xin, O. Gang, E. B. Zhulina, M. Rubinstein, and E. Kumacheva, Surface

patterning of nanoparticles with polymer patches, Nature (London) **538**, 79 (2016).

[3] W. Liu, M. Tagawa, H. L. Xin, T. Wang, H. Emamy, H. Li, K. G. Yager, F. W. Starr, A. V. Tkachenko, and O. Gang, Diamond family of nanoparticle superlattices, Science **351**, 582 (2016).

[4] P. Akcora, H. Liu, S. K. Kumar, J. Moll, Y. Li, B. C. Benicewicz, L. S. Schadler, D. Acehan, A. Z. Panagiotopoulos, V. Pryamitsyn, V. Ganesan, J. Ilavsky, P. Thiyagarajan, R. H. Colby, and J. F. Douglas, Anisotropic self-assembly of spherical polymer-grafted nanoparticles, Nat. Mater. **8**, 354 (2009).

[5] P. F. Damasceno, M. Engel, and S. C. Glotzer, Predictive self-assembly of polyhedra into complex structures, Science **337**, 453 (2012).

[6] J. Cai, C. Lv, and A. Watanabe, Facile preparation of hierarchical structures using crystallization-kinetics driven self-assembly, ACS Appl. Mater. Interfaces **7**, 18697 (2015).

[7] D. Zhao, V. Gimenez-Pinto, A. M. Jimenez, L. Zhao, J. Jestin, S. K. Kumar, B. Kuei, E. Gomez, A. S. Prasad, L. S. Schadler, M. M. Khani, and B. C. Benicewicz, Tunable multiscale nanoparticle ordering by polymer crystallization, ACS Cent. Sci. **3**, 751 (2017).

[8] V. J. Anderson, E. M. Terentjev, S. P. Meeker, J. Crain, and W. C. K. Poon, Cellular solid behaviour of liquid crystal colloids 1. Phase separation and morphology, Eur. Phys. J. E **4**, 11 (2001).

[9] V. J. Anderson and E. M. Terentjev, Cellular solid behaviour of liquid crystal colloids 2. Mechanical properties, Eur. Phys. J. E **4**, 21 (2001).

[10] P. G. Petrov and E. M. Terentjev, Formation of cellular solid in liquid crystal colloids, Langmuir **17**, 2942 (2001).

[11] S. T. Riahinasab, A. Keshavarz, C. N. Melton, A. Elbaradei, G. I. Warren, R. L. B. Selinger, B. J. Stokes, and L. S. Hirst, Nanoparticle-based hollow microstructures formed by two-stage nematic nucleation and phase separation, Nat. Commun. **10**, 894 (2019).

[12] D. R. Uhlmann, B. Chalmers, and K. A. Jackson, Interaction between particles and a solid-liquid interface, J. Appl. Phys. **35**, 2986 (1964).

[13] Ch. Körber, G. Rau, M. D. Cosman, and E. G. Cravalho, Interaction of particles and a moving ice-liquid interface, J. Cryst. Growth **72**, 649 (1985).

[14] S. A. Barr and E. Luijten, Structural properties of materials created through freeze casting, Acta Mater. **58**, 709 (2010).

[15] See Supplemental Material at http://link.aps.org/supplemental/10.1103/PhysRevE.105.L032601 for snapshots for the final state of particles in a suspension after its medium crystallizes at different speeds (Fig. S1); fitting parameters for studies on solvent size, particle size and Hamaker constant (Tables S1–S3). Analysis of equilibrium distance between particle and crystal front (Figs. S2–S4).

[16] S. Plimpton, Fast parallel algorithms for short-range molecular dynamics, J. Comput. Phys. **117**, 1 (1995).

[17] D. Langbein, in *Intermolecular Forces,* edited by B. Pullman (Springer, Dordrecht, 1981), pp. 547–562.

[18] M. E. Mackay, T. T. Dao, A. Tuteja, D. L. Ho, B. Van Horn, H.-C. Kim, and C. J. Hawker, Nanoscale effects leading to non-Einstein-like decrease in viscosity, Nat. Mater. **2**, 762 (2003).